Improved Handling Qualities for the OH-58D Kiowa Warrior in the Degraded Visual Environment

Tom Berger
University Affiliated Research Center (UCSC)
NASA Ames Research Center
Moffett Field, CA, USA

Mark B. Tischler
Chris L. Blanken
Brian T. Fujizawa
Aeroflightdynamics Directorate (AMRDEC)
U.S. Army Research, Development and Engineering Command
Moffett Field, CA, USA

Jeffrey W. Harding
Harding Consulting, Inc.
Kennesaw, GA, USA

Christopher C. Borden
Aviation Engineering Directorate (AMRDEC)
U.S. Army Research, Development and Engineering Command
Redstone Arsenal, AL, USA

Larry E. Cothren
CW5 James J. Wright
Aviation Flight Test Directorate (DTC)
U.S. Army Test and Evaluation Command
Fort Rucker, AL, USA

David R. Arterburn
Matthew R. Pfrommer
Kiowa Warrior PMO (ASH PO)
U.S. Army Program Executive Office, Aviation
Redstone Arsenal, AL, USA

An OH-58D flight dynamics and control system model has been developed in preparation for a potential flight control system upgrade towards meeting Aeronautical Design Standard ADS-33E-PRF criteria for the Kiowa Warrior Cockpit and Sensor Upgrade Program. Frequency sweep and trim flight data, collected at hover and 80 kts, were collected for simulation model development and validation. The data were used to identify a six degree-of-freedom state space model of the OH-58D. The current OH-58D Rate Command stability and control augmentation system, which was developed by hand tuning the control law gains during flight test, was improved using the newly developed model. Retaining the existing control law architecture, several improved gain sets were generated by utilizing a multi-objective parametric optimization approach to arrive at control law parameters that concurrently satisfy all system requirements. A Level 1 Rate Command response type system was optimized. Additionally, previously unused lagged-rate gains in the control laws were used to generate several short-term Attitude Command Attitude Hold response type configurations in order to meet ADS-33E response type requirements for degraded visual environments in the short-term response. After a down select flight test to pick one of the short-term Attitude Command Attitude Hold gain sets, a limited handling qualities assessment was flown in the DVE to compare the current Rate Command control laws with the optimized short-term Attitude Command Attitude Hold control laws.

Presented at the American Helicopter Society 67th Annual Forum, Virginia Beach, Virginia, May 3-5, 2011.

Fig. 1. OH-58D Kiowa Warrior in flight

Introduction

The Bell OH-58D Kiowa Warrior (KW), shown in Figure 1, is the U.S. Army's primary armed reconnaissance aircraft. It is a single-engine, four-bladed helicopter with a distinctive mast mounted site (MMS) which houses a suite of imaging and range finding sensors, providing the KW with target acquisition and designation capabilities in both day and night. The KW entered Army service in 1985, and since then has seen several modifications to its Rate Command (RC) stability and control augmentation system (SCAS) gains. The most recent of these was completed in 2005 and was done by the arduous task of hand tuning SCAS gains during flight test (Ref. 1).

Since the beginning of Operations Enduring Freedom and Iraqi Freedom, Kiowa Warriors have flown over 500,000 combat hours (Ref. 2). During that time, the majority of incidents resulting in aircraft loss among Army helicopters have occurred in the hover/low speed regime and of those, the majority were caused by a degraded visual environment (DVE) (Ref. 3). The Study on Rotorcraft Safety and Survivability (Ref. 3) lists advanced flight control systems and modern control laws that affect rotorcraft handling qualities as a key solution to mitigate rotorcraft losses. The benefit of additional augmentation for improved safety in the DVE was recently seen in the CH-47F Digital Advanced Flight Control Systems (DAFCS) (Ref. 4) and UH-60M Upgrade (Ref. 5). This is in line with Aeronautical Design Standard ADS-33E-PRF, which requires increased augmentation to achieve Level 1 handling qualities as the visual environment degrades (Ref. 6), specifically, requiring an Attitude Command Attitude Hold (ACAH) response type for the DVE, which the current OH-58D does not have.

The Kiowa Warrior's partial authority (roughly $\pm 10\%$) RC flight control system has provided sufficient control sensitivity for combat operations while providing sufficient stability for day, night, and night vision goggles (NVGs) armed reconnaissance mission in visual meteorological conditions. The KW Cockpit and Sensor Upgrade Program (CASUP) is focused on mission equipment upgrades including the removal of the MMS and integration of a modern nose mounted sensor (NMS) to improve the Kiowa Warrior's stand-off distance for reconnaissance and targeting. While the KW CASUP requires no flight control improvements to meet the requirements of the capabilities design document (CDD), the change in mass moment of inertia resulting from removal of the MMS may require some optimization of the SCAS gains to improve handling qualities in the new configuration. The KW PM elected to invest in the development and validation of a flight control modeling effort to reduce flight test costs associated with optimizing SCAS gains during flight test and to provide a validated model from which future flight control improvements within the current flight control hardware configuration could be evaluated. In support of this, a flight dynamics and control system model of the OH-58D was developed. This opportunity was used to rapidly develop an improved SCAS for the OH-58D using the Control Designer's Unified Interface (CONDUIT®) with the goal of demonstrating an upgraded SCAS that meets the ACAH requirement of ADS-33E in the short-term, in support of future upgrades.

Thus, this project has two main objectives. First, to develop a validated simulation model to support flight control improvements. This involved using flight test data to validate and update an existing analysis model of the OH-58D.

Second, to demonstrate the feasibility and advantages of improved control laws for the OH-58D, using the flight dynamics model. This included developing both a Level 1 RC response type system, as well as a short-term ACAH response type system in order to meet ADS-33E response type criteria for a DVE in the short-term response only, while maintaining the current SCAS architecture.

This paper will cover the development of the analysis and simulation model, the flight testing program, the model identification and validation, the control law analysis and optimization, and the results of the handling qualities flight testing, as well as a discussion of the results.

System Overview

Figure 2 shows a simplified schematic of the OH-58D control laws block diagram. Pilot stick inputs are fed into both a mechanical mixer (1) and the SCAS (2). SCAS outputs are mixed and drive the limited authority SCAS actuators (3). The SCAS actuator outputs are subtracted from the mixed pilot stick commands, and the total is used to drive the boost actuators (4). The boost actuators drive the swashplate (5), which in turn drives the bare-airframe (6). Finally, the rates from the bare-airframe are fed back to the SCAS. Each part of this block diagram was validated from flight test and rigging data individually, and finally the entire block diagram was validated as a whole.

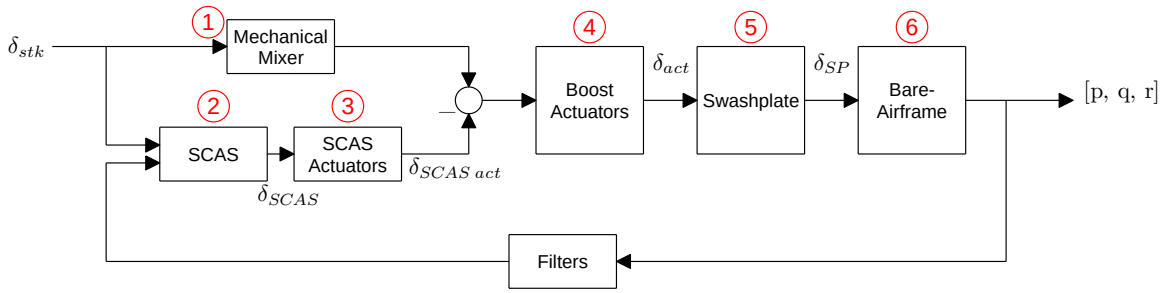

Fig. 2. Simplified schematic of the OH-58D control laws block diagram

Stability and Control Augmentation System

The current OH-58D SCAS ((2) in Figure 2) is a three-axis (pitch, roll, and yaw), limited-authority, digital system with a heading-hold mode. SCAS authority in each axis is limited to roughly $\pm 10\%$ control movement. Each axis includes an angular rate feedback loop for stability augmentation and a control input feed-forward loop for control power augmentation. In addition, each of the three axes has an overall signal amplifier gain and a previously unused lagged-rate feedback gain, which is of particular interest to this project. The lagged-rate gain, equivalent to washed-out attitude, was used to achieve a short-term ACAH response. The SCAS gains are scheduled across two airspeed regimes, with a low airspeed set (between 0 and 40 kts) and a high airspeed set (60 kts and above). There is a linear transition of the gains between the two airspeed regime sets. This effort is concerned with the low airspeed set only.

The currently flying set of gains was optimized by hand tuning the overall signal amplifier gain of each axis in flight (Ref. 1).

Flight Testing Program

Flight Test Instrumentation

Flight testing was done on an instrumented OH-58D aircraft. The aircraft was flown with doors on, .50-caliber machine gun (left), M261 rocket pod (right), and MMS on, with an average gross weight of about 5000 lbs. Pilot stick inputs, as well as boost actuator positions were recorded. Boost actuator positions were used to reconstruct swashplate angles, which were used as the input to the bare-airframe model developed. This was done using an actuator to swashplace mixing matrix ((4) to (5) in Figure 2) which was identified from a hanger rigging check of the aircraft. Aircraft angular rates and attitudes and vertical acceleration were recorded from the aircraft bus. Angular rates and attitudes were also recorded from an on board C-MIGITS (Miniature Integrated GPS/INS Tactical System) unit, as were linear accelerations (corrected to the c.g.) and North, East, Down (NED) velocities. Finally, air data in the form of total velocity, angle of attack, and angle of sideslip were recorded from a nose mounted boom.

Testing Methods

Flight testing was done in four phases, described below.

Phase 1 Previous SCAS improvement effort (Ref. 1). Data from this phase, in the form of pulse and step responses, were used to develop an initial bare-airframe model which was used for preliminary flight control design. Recorded pilot stick inputs and SCAS actuator positions were used to reconstruct swashplate angles (output of (5) in Figure 2), as neither the swashplate nor the boost actuators were instrumented in the previous SCAS improvement effort. An example of a reconstructed lateral swashplate angle, A_1, and the resulting aircraft roll rate, p, are shown in Figure 3. These data were analyzed in CIFER®, using the methods presented in Tischler and Remple (Ref. 7), and on-axis first-order transfer function models of the aircraft were identified.

Phase 2 Control law comparison and down select. During the control law comparison and down select flight, pilots flew the different optimized control laws in a GVE in back-to-back qualitative comparisons to down select which configuration to test in the DVE. Pilots flew the Hover, Sidestep, and Acceleration/Deceleration mission task elecments (MTEs) from ADS-33E (Ref. 6). No formal handling qualities ratings were collected, but qualitative comments were used to perform a SCAS gain set down select.

Phase 3 Model validation data collection. During this phase, frequency sweeps and doublets were flown in each of the four control axes at both an out of ground effect hover and level flight at 80 kts. The frequency sweeps followed the flight test technique guidance contained in (Ref. 7). The doublets were flown to provide time history data for model verification purposes. Additionally, axial trim, longitudinal static stability, and sideward trim data were collected. During this effort, boost actuator

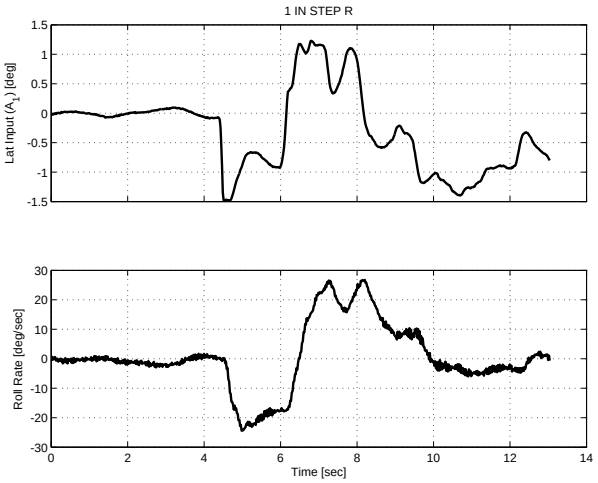

Fig. 3. Example lateral input (A_1) and output (p) data used for preliminary system identification

positions (output of (5) in Figure 2) were recorded. They were used to reconstruct swashplate angles based on mixing matrices identified during a hanger rigging check of the aircraft. An example of a reconstructed lateral swashplate angle and the resulting aircraft roll rate from a frequency sweep maneuver are shown in Figure 4.

Phase 4 Control law handling qualities assessment in DVE. This phase is described in detail in the Handling Qualities Flight Testing section below.

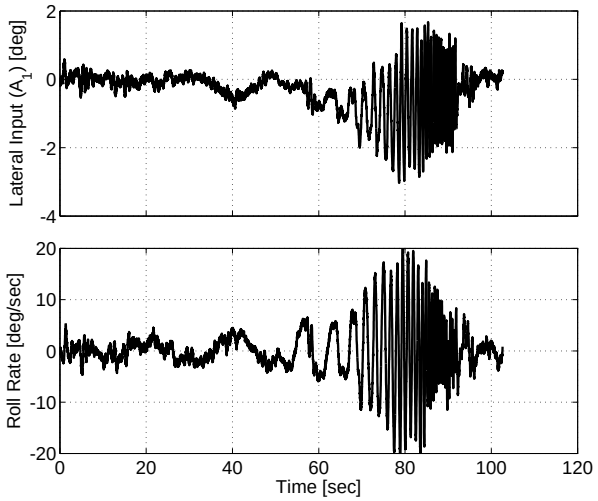

Fig. 4. Example lateral input (A_1) and output (p) data used for final system identification

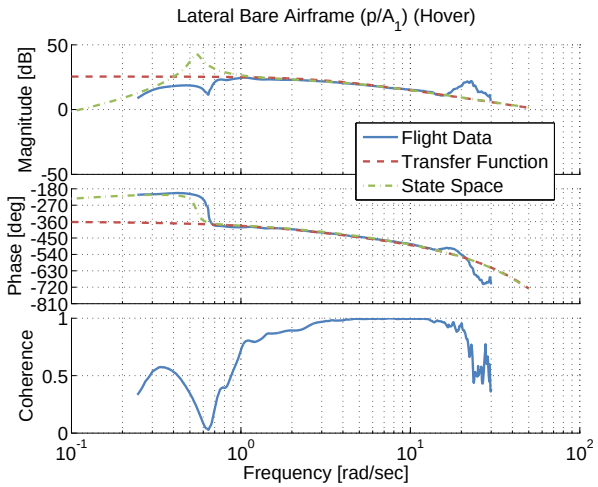

Fig. 5. Lateral frequency response (p/A_1) from CIFER® with initial transfer function model and final state-space model overlay

Model Identification and Validation

Bare Airframe Model Identification

In order to produce meaningful analyses and develop a good control system, an accurate model of the aircraft dynamics ((6) in Figure 2) is necessary. Initially, existing flight test data of the OH-58D from the previous SCAS improvement effort (Ref. 1), in the form of pulse and step responses, were used to develop on-axis transfer function models of the pitch, roll, and yaw responses of the aircraft. This was done using the Comprehensive Identification from FrEquency Responses (CIFER®) software (Ref. 7). The models were identified from swashplate inputs. Figure 3 shows one of the lateral axis input and output data sets used for the initial transfer function model identification. Figure 5 shows the corresponding frequency response as well as the transfer function model that was matched to it (in units of deg/sec per deg of swashplate deflection), given by the following equation:

$$\frac{p}{A_1} = \frac{55.94}{s+3.35} e^{-0.096s} \tag{1}$$

Overlaid on the figure is also the response of the final state-space model, which is described in the next section. The match between the flight data and the first order transfer function is quite good in the frequency range of 1-10 rad/sec, with a fit cost of 26.2. Costs less than 50 indicate nearly perfect agreement (Ref. 7). Figure 6 shows a doublet response from flight, and of the transfer function model. There is an excellent agreement between the two responses. As with the frequency response, there is also an overlay of the response of the final state-space model described below. Similar transfer function models were generated for the pitch rate and yaw rate responses.

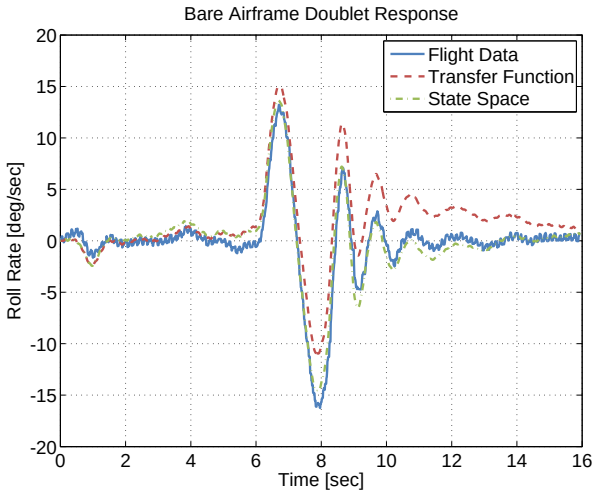

Fig. 6. Roll rate doublet response from flight and from the initial transfer function model and final state-space model

As new data were gathered, first from a data consistency check flight, and then from the frequency sweep flights, updated models were identified. The updated models were used to validate the ones which were used for SCAS gain optimization, and to re-evaluate the optimized control laws. In each iteration of the model identification, the models used for SCAS gain optimization were deemed valid, and re-optimization of the SCAS gains was not necessary. The final phase of model development resulted in a six degree-of-freedom state-space model of the bare airframe, described below.

State-Space Model Identification

Using the methods presented in Tischler and Remple (Ref. 7), CIFER® was used to identify a six degree-of-freedom state-space model of the bare-airframe dynamics using frequency sweep data, static-stability trim data, and doublet data. The states of the identified model are the aircraft translational velocities, angular rates, and angular attitudes in units of ft/sec, rad/sec, and rad, respectively. Through the identification process, it was found that the aircraft dynamics were largely decoupled for inputs at the swashplate resulting in the identification of on-axis stability and control derivatives only as shown in Table 1 (the N_v parameter was identified from static-stability trim data and held fixed in the model). The low Cramer-Rao bounds (nearly all <20%) show the good reliability of the identified parameters (Ref. 7).

A comparison of the state-space model and transfer function model to the flight data, for the bare airframe roll axis, can be seen in Figure 5. The state-space model is seen to agree with the flight data down to a lower frequency than the transfer function model. This can also be seen in Figure 6, which shows a doublet response from flight, and of the state-space and transfer function models. The state-space model is seen to have less drift from the flight data than the transfer function model.

Table 1. Final state-space and transfer function models

	ID Model			TF Model
Param.	Value	C.R. (%)	Insens. (%)	Value
		F-matrix		
X_u	-0.01000[a]	.....	.....	-0.01000
X_q	2.562	17.04	6.668	0.000
Y_v	-0.1469[a]	.....	.....	-0.1469
Y_p	-0.9258	31.22	9.889	0.000
Z_w	-0.2492	12.77	5.825	-0.2492
L_v	-0.03644[a]	.....	.....	0.000
L_p	-3.819	7.120	1.740	-3.349
M_u	0.01444[a]	.....	.....	0.000
M_q	-1.248	7.103	2.548	-1.238
N_v	0.01488[a]	.....	.....	0.000
N_r	-1.128	19.36	7.694	-1.165
		G-matrix		
X_{B_1}	0.6632	4.052	1.752	0.000
Y_{B_1}	0.6496	6.247	2.177	0.000
Z_{θ_0}	-3.854	4.253	1.941	-3.854
L_{A_1}	1.034	5.118	1.349	0.9736
M_{B_1}	-0.2101	3.189	1.273	-0.2204
$N_{\theta_{tr}}$	0.1501	4.606	2.116	0.1558
τ_{A_1}	0.09815	7.802	2.880	0.09620
τ_{B_1}	0.07735	8.172	3.637	0.08660
τ_{θ_0}	0.000[b]	.....	.....	0.000
τ_{tr}	0.04443	20.03	8.469	0.03730

a Fixed parameters in model structure
b Eliminated from model structure

The values presented in Table 1 differ from those presented in (Ref. 8) in which an OH-58D bare airframe model was identified for inputs at the pilot stick. Of particular interest is the differences related to effective roll flapping spring, $L_{\beta_{1s}}$. The $L_{\beta_{1s}}$ value for the newer model is given by the following equation (Ref. 7):

$$L_{\beta_{1s}} = \frac{L_p}{\tau_{A_1}} = -38.91 \tag{2}$$

compared to $L_{\beta_{1s}} = -53.06$ in the earlier work. In the previous test, the aircraft weight was 4800 lbs and the aircraft was in a clean configuration, for the most recent tests, the aircraft weight was 5120 lbs and had a side mounted rocket-pod and machine gun. Using the following relationship between $L_{\beta_{1s}}$ and aircraft and rotor data:

$$-L_{\beta_{1s}} = \frac{W h_r}{I_{xx}} + \frac{n_b M_\beta \Omega^2 e}{2 I_{xx}} + \frac{n_b K_\beta}{2 I_{xx}} \tag{3}$$

and data from (Ref. 9), it was determined that an inertia scale factor of 1.3 was needed to account for the change in

Table 2. Cost functions for state-space and transfer function models

Response	ID Model	TF Model
$\dot{v}/A_1$	20.005	34.394
p/A_1	14.367	3.481
a_y/A_1	63.892	10097.925
$\dot{u}/B_1$	42.199	145.499
q/B_1	25.474	14.854
a_x/B_1	25.606	53666.559
a_z/θ_0	5.845	5.845
r/θ_{tr}	95.994	100.829
Average	36.673	8008.798

Table 3. Cost summary table for state-space and transfer function models

Control Axis	ID Model	TF Model
A_1	0.884	1.150
B_1	1.315	2.325
θ_0	0.335	0.335
θ_{tr}	0.685	0.939

$L_{\beta_{1s}}$ which is consistent with the weight distribution and additional aircraft components of the most recent flight tests.

Figure 7 compares the frequency responses of the identified state-space model and preliminary transfer function model with the flight data. Notice that the transfer function model does not capture the a_x and a_y responses. This is reflected in Table 2 which compares the model accuracy based on the frequency domain fit cost. Generally, a cost under 100 is considered a good match between the model and the flight data while a cost under 50 is considered excellent. As seen in Table 2, the identified state-space model has a significantly lower cost than the transfer function model.

Figure 8 plots the time domain verification results of a lateral piloted doublet from the identified state-space model and the preliminary transfer function model. Notice there is some minor off-axis pitch and yaw response which is not captured by the model. This is a result of the fact that the off-axis stability and control derivatives could not be identified due to the low off-axis energy content of the frequency sweeps.

Table 3 shows the RMS fit error between the models and flight data; lower RMS fit costs reflect higher levels of predictive accuracy with a value less than 1 indicating very good predictive accuracy. The values presented in Table 2 and Table 3 both show that the identified state-space model is a more accurate representation of the aircraft bare-airframe dynamics.

Analysis Model Validation

The state-space model was used in place of the first order transfer functions for the control law analysis and fixed based simulation. Once the validated bare airframe model was integrated into the block diagram, the entire analysis model could be validated. First, the mixing between pilot stick and boost actuators ((1) to (4) in Figure 2) and between boost actuators and swashplate angles ((4) to (5) in Figure 2) was validated against rigging data. Figure 9 shows swashplate angles measured during the rigging check versus swashplate angles from the analysis model for different cyclic and collective stick configurations. Listed on the figure are the RMS error between the two curves for each measurement. It shows a nearly perfect agreement between the mixing in the analysis model and the rigging data.

Next, the SCAS model was validated by comparing the measured SCAS activity from flight during a particular maneuver with that of the SCAS model, by simulating it with the pilot stick and aircraft rates from flight. Figure 10 shows the pitch, roll, and yaw SCAS activity for a roll doublet manuever from flight data and from the model. There is an excellent agreement between the model and flight data, indicating correct modeling of the SCAS.

Finally, the entire analysis model was validated. This was done by looking at both closed- and broken-loop frequency responses. Figure 11 shows the closed-loop response obtained from flight and from the analysis model, using both the initial transfer function bare-airframe model used for flight control design, and the final state-space model used for analysis of the optimized control laws. The response from flight was obtained by analyzing frequency sweep flight data in CIFER®. The response from the analysis model was obtained by simulating the model with the same pilot input used in flight, and analyzing the resulting data in CIFER®. This was done instead of extracting a frequency response from the linearized model in order to capture limiting effects of the SCAS and actuators. The figure shows excellent agreement between flight data and both the transfer function and state-space models. As expected, the state-space model agrees with flight across a larger frequency range, but the initial transfer function model is a faithful representation of the aircraft in the frequency range of greatest interest for handling qualities assessment and flight control design, 1-10 rad/sec.

Figure 12 shows the broken-loop response from flight and from the analysis model using both the initial transfer function model as well as the final state-space model. The broken-loop response from flight was obtained by multiplying the bare-airframe response from flight by the frequency response of the SCAS model, which was previously validated. Again, there is near perfect agreement between the responses, validating the analysis model with both the initial transfer function model used for flight control optimization and the final state-space model used for flight control

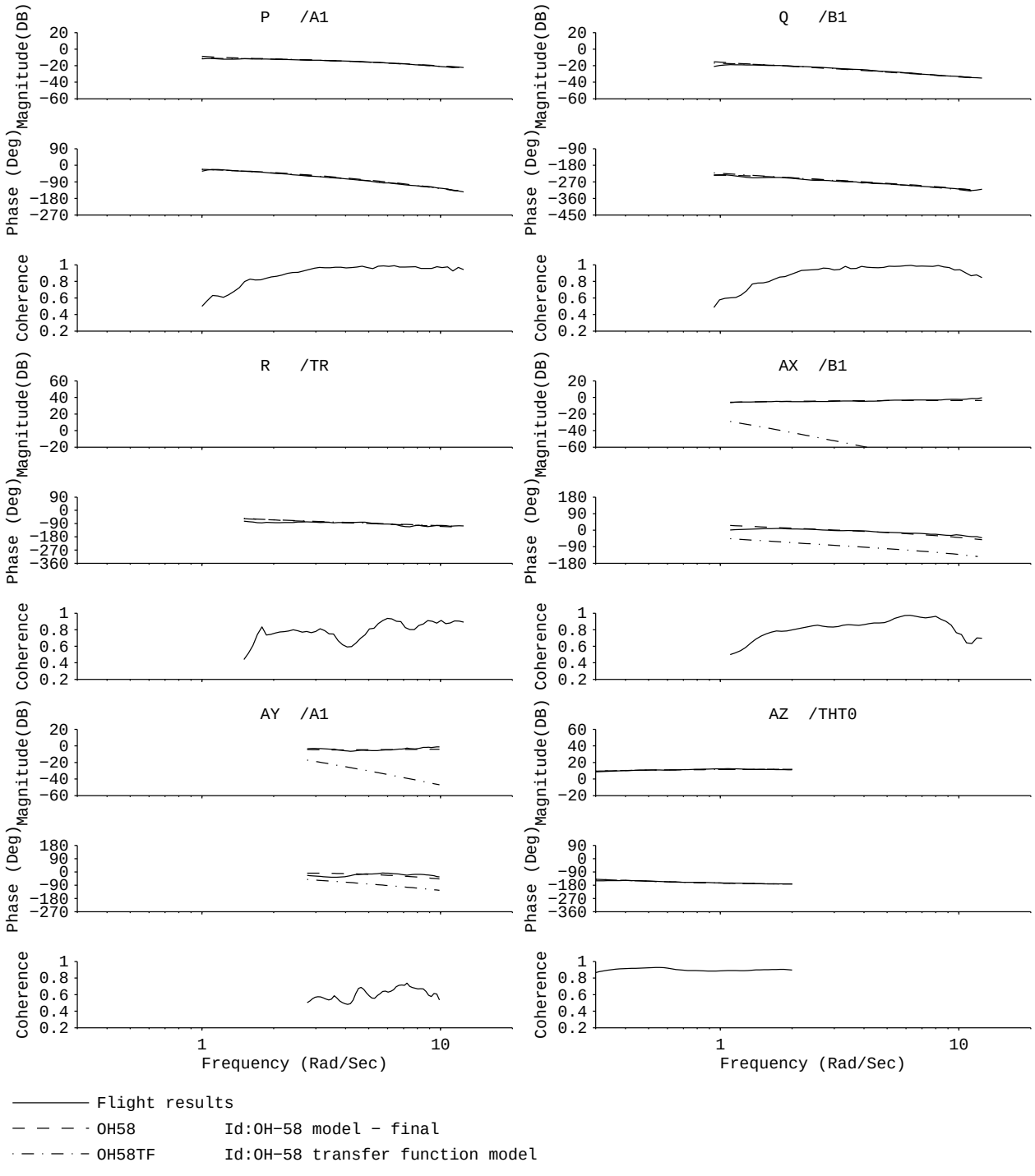

Fig. 7. Frequency domain comparison of identified state-space model and transfer function model

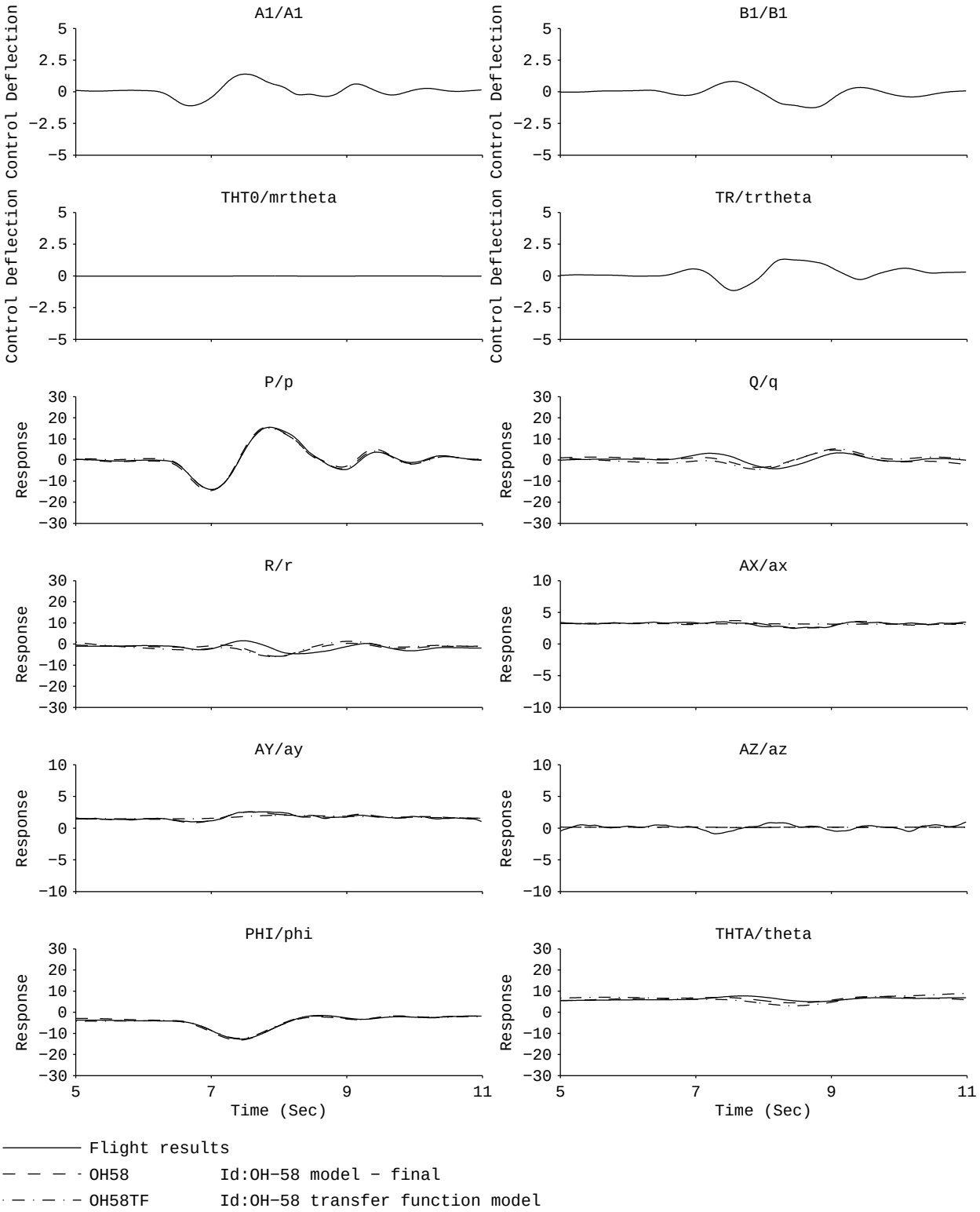

Fig. 8. Time domain comparison of identified state-space model and transfer function model

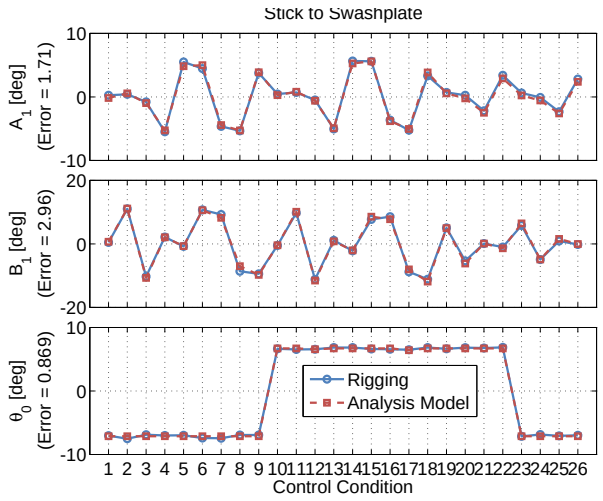

Fig. 9. Measured and modeled swashplate angles for different pilot stick positions

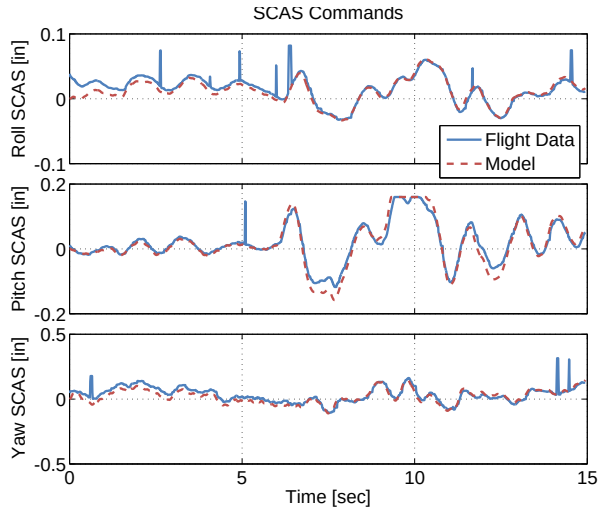

Fig. 10. SCAS commands from flight and analysis model

and handling qualities analysis.

Control Law Analysis and Optimization

Control Designer's Unified Interface

Control law analysis and optimization was done using the Control Designer's Unified Interface (CONDUIT®) (Ref. 10). CONDUIT® is a commercial software tool developed by the U.S. Army Aeroflightdynamics Directorate in conjunction with the University Affiliated Research Center (UCSC). It allows for evaluation of a Simulink block diagram against a defined set of stability, handling qualities, and performance specifications, and performs a multi-modal parametric optimization of user defined parameters in the block diagram (e.g. SCAS gains) in order to meet those specifications.

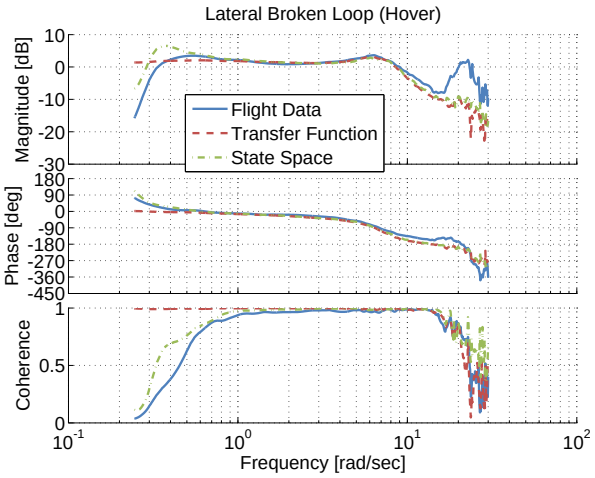

Fig. 11. Closed-loop roll rate response from flight data, the initial transfer function model, and the final state-space model

Specifications

A comprehensive set of stability, handling qualities, and performance specifications was chosen to drive the optimization of the control laws. The handling qualities specifications are based on ADS-33E (Ref. 6). The required stability margin is based on the military specification for flight control systems, MIL-DTL-9490E (Ref. 11).

Specifications are divided into three constraint types in CONDUIT®. Specifications that ensure aircraft stability, such as the eigenvalue, stability margin, and Nichols margin specifications, are categorized as hard constraints. These specifications are met during the first phase of optimization. Next are the handling qualities specifications, such as piloted bandwidth, response damping, disturbance rejection

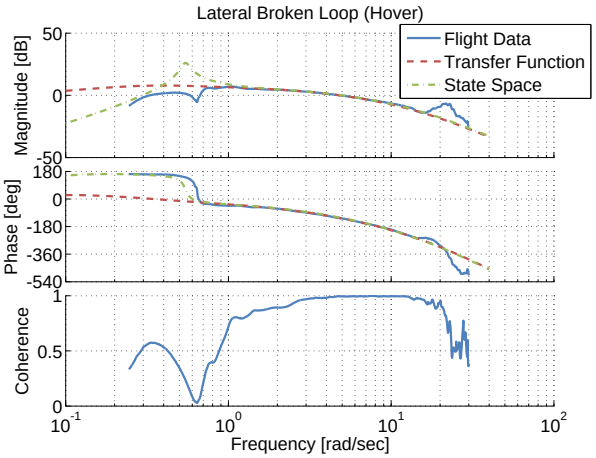

Fig. 12. Broken-loop responses from flight, the analysis model with the initial transfer function model, and the analysis model with the final state-space model

bandwidth, and the Open Loop Onset Point criteria, which limits actuator rate saturation. These specifications are categorized as soft constraints, and are met during the second phase of optimization. Finally, there are the performance specifications, such as actuator root mean squared (RMS) and crossover frequency, categorized as summed objective constraints. Once all other specifications are met, the optimization attempts to minimize this set in the third phase of optimization. This last phase is done to achieve a design that meets all of the specifications, but does so with the minimum necessary actuator usage and crossover frequency. Table 4 lists the specifications used for analysis and optimization.

Analysis of Previously Flown Designs

Before optimization was carried out, the configurations flown in the previous SCAS improvement effort (Ref. 1) were evaluated and the resulting predicted handling qualities were correlated with recorded pilot comments. In that effort, five SCAS gain configurations were flown–a baseline configuration, two configurations with the overall signal amplifier gain in each SCAS 50% and 100% higher than the baseline, and two configurations with the overall signal amplifier gain in each SCAS 25% and 50% lower than the baseline. An example of the correlation between predicted handling qualities from CONDUIT® and the pilot comments for three of the configurations is shown in Figure 13. As the phase margin decreases from 85 deg in pitch and 146 deg in roll in Configuration 3 to 40 deg in pitch and 52 deg in roll in Configuration 4, pilots described Configuration 4 as "more twitchy" As the phase margin further decreased to 27 deg in pitch and 21 deg in roll in Configuration 5, pilots described the configuration as "objectionable." Figure 14 shows the decrease in damping associated with the decrease in phase margin between Configurations 3 and 4. This analysis shows the right trends in handling qualities between gain sets, further validating the model used.

Improved Rate Command Design

A design which maintains the aircraft's RC response type but meets the Level 1 handling qualities requirements was developed first. The objective of the optimized RC design was to increase the stability margin and damping of the aircraft, while reducing the crossover frequency. Tables 5 and 6 lists the values of the specifications for the baseline and optimized RC designs. Figures 15 through 18 show time- and frequency-domain comparisons in the Roll axis between the baseline design and the optimized RC design. Figure 15 shows a pilot stick pulse response of the two configurations. It clearly shows the increase in damping of the optimized RC design versus the baseline design, as well as a decrease in SCAS activity. This can also be seen in the roll rate disturbance pulse response in Figure 16. Figure 17

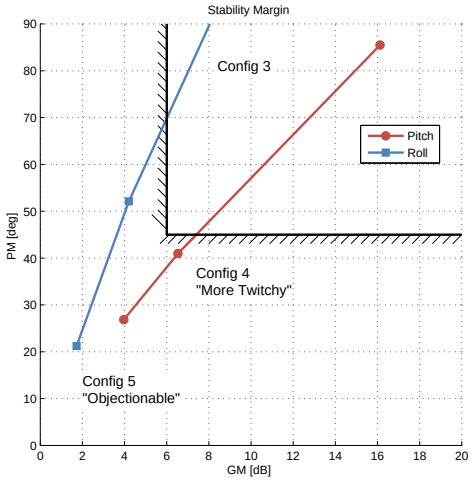

Fig. 13. Stability margins of three of the SCAS gain configurations flown in (Ref. 1)

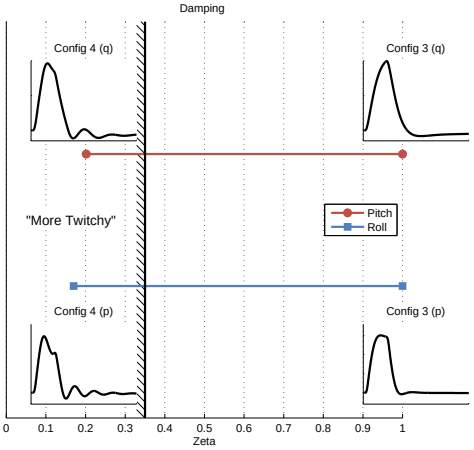

Fig. 14. Damping of two of the SCAS gain configurations flown in (Ref. 1)

shows the closed-loop frequency response of the two designs. Again, the increase in damping can be seen at around 7 rad/sec, where the optimized RC design response is missing the "hump" that is evident in the frequency response of the baseline design. Figure 18 shows the broken-loop response of the two configurations, and shows the decrease in crossover frequency and increase in stability margin of the optimized RC design. A similar trend of increased damping and decreased crossover frequency was seen in the Pitch axis, which can be seen in Table 6.

Short-Term Attitude Command Attitude Hold Designs

Next, the lagged-rate gains in the Pitch and Roll SCASs were used to give the aircraft short-term ACAH capabilities. Lagged-rate gains were used because of the requirement to stay within the current SCAS architecture and the lack of pure attitude feedbacks in the current SCAS. Lagged-rate gains are equivalent to washed-out attitude gains, and hence the short-term aspect of the ACAH capabilities, as the abil-

Table 4. SCAS Optimization Specifications

Constraint	Spec Name	Description	Axis
Hard	EigLcG1	Eignevalues in L.H.P	-
	StbMgG1	Gain Phase Margin (6 dB, 45 deg)	Pitch, Roll, Yaw, HH
	NicMgG1	Robust Margins	Pitch, Roll, Yaw, HH
Soft	BnwAtH1	Bandwidth (Other MTEs, UVE > 1)	Pitch, Roll
	BnwYaH2	Bandwidth (Other MTEs)	Yaw, HH
	DstBwG1	Disturbance Rejection Bandwidth	ϕ, θ, ψ (HH)
	DstPkG1	Disturbance Rejection Peak	ϕ, θ, ψ (HH)
	EigDpG1	Eigenvalue Damping (Below Piloted BW)	-
	EigDpG1	Eigenvalue Damping (Above Piloted BW)	-
	OlpOpG1	Open Loop Onset Point (Actuator Rate Limiting)	Pitch, Roll, Yaw, HH
	CrsMnG1	Minimum Crossover Frequency	Pitch, Roll, Yaw, HH
	DmpTmG1	Time Domain Damping (Pilot Input)	Pitch, Roll, Yaw, HH
	DmpTmG1	Time Domain Damping (Disturbance Input)	Pitch, Roll, Yaw, HH
Summed Obj.	CrsLnG1	Crossover Frequency	Pitch, Roll, Yaw, HH
	RmsAcG1	Actuator RMS	Pitch, Roll, Yaw, HH

Table 5. Lateral Handling Qualities Comparison

	Baseline	Optimized RC	Lo stACAH	Hi stACAH	Qk stACAH
ω_c [rad/sec]	5.0	1.2	2.3	2.8	2.5
PM [rad/sec]	57.8	142.0	74.4	65.2	69.7
GM [dB]	5.1	12.3	10.4	8.6	9.9
BW_{phase} [rad/sec]	4.1	3.5	4.0	4.4	4.0
BW_{gain} [rad/sec]	2.5	3.4	3.6	3.2	3.1
ζ [-]	0.21	0.51	0.53	0.44	0.51
p-DRB [rad/sec]	4.0	2.4	3.3	3.6	3.4
p-DRP [dB]	8.9	5.9	3.1	4.0	3.3
ϕ-DRB [rad/sec]	-	-	0.99	1.1	1.1
ϕ-DRP [dB]	-	-	2.4	3.0	2.7

ity of the SCAS to command and hold an attitude is washed-out in steady state. For this optimization, the attitude disturbance rejection bandwidth (DRB) and disturbance rejection peak (DRP) specifications were added (Ref. 10). Additionally, the piloted bandwidth specification was evaluated for an ACAH system, i.e. the bandwidth frequency was taken to be the phase bandwidth, and not the lower of the phase and gain bandwidths. However, the gain bandwidth was still evaluated to ensure that it did not drop far below the phase bandwidth, which may cause the aircraft to become PIO prone (Ref. 6).

The objective for the short-term ACAH design was to have a good disturbance rejection characteristics, while maintaining reasonable stability margins, crossover frequency, and actuator usage. This was done by incrementally increasing the DRB and crossover frequency requirements of the design and producing an optimized design at each point. This method of design margin optimization is described in more detail in (Ref. 10), (Ref. 12), and (Ref. 13). A secondary requirement was to maintain Level 1 quickness, which the baseline design has. This was addressed by generating two families of optimized designs–one in which only the lagged-rate and rate gains were modified (from which the "Hi" and "Lo" designs were selected), and a higher quickness family in which an additional feed forward stick gain, which is zero in the baseline design, was allowed to vary (from which the "Qk" design was selected).

Figures 19(a) through 19(e) show the varying handling qualities and SCAS gains of the two short-term ACAH families of cases plotted versus crossover frequency. Figure 19(d) shows the monotonic increase in DRB of the designs, as that requirement was increased for each point. Figure 19(a) shows the associated loss of phase margin with increased DRB (Ref. 10) and (Ref. 13). The increase in DRP with increase in DRB, as dictated by the Bode integral theorem, which states that a sensitivity reduction in one frequency range comes at the expense of sensitivity increase at another (the "waterbed effect"), can be seen in Figure 19(e). The increasing values in lagged-rate (i.e. attitude) gain in order to achieve an increase in DRB and slight de-

Table 6. Longitudinal Handling Qualities Comparison

	Baseline	Optimized RC	Lo stACAH	Hi stACAH
ω_c [rad/sec]	3.6	1.4	1.7	2.0
PM [rad/sec]	41.0	86.5	57.5	56.5
GM [dB]	6.5	16.9	14.0	12.1
BW_{phase} [rad/sec]	2.6	1.8	2.0	2.2
BW_{gain} [rad/sec]	1.9	2.2	2.4	2.1
ζ [-]	0.31	0.75	0.54	0.68
q-DRB [rad/sec]	2.5	1.4	1.8	2.3
q-DRP [dB]	9.1	14.1	2.6	2.9
θ-DRB [rad/sec]	-	-	0.62	0.72
θ-DRP [dB]	-	-	2.8	4.3

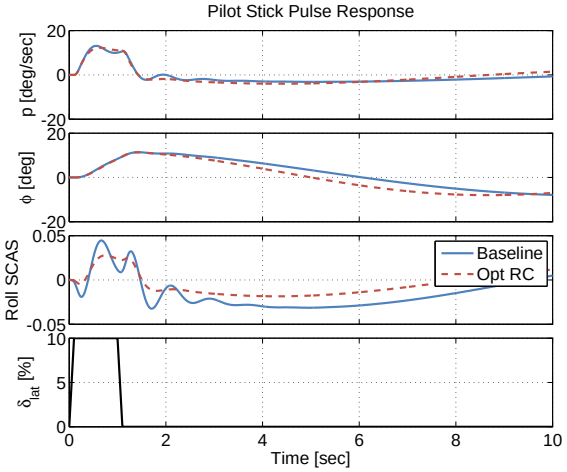

Fig. 15. Lateral pilot stick pulse response for the baseline and optimized RC gain configurations

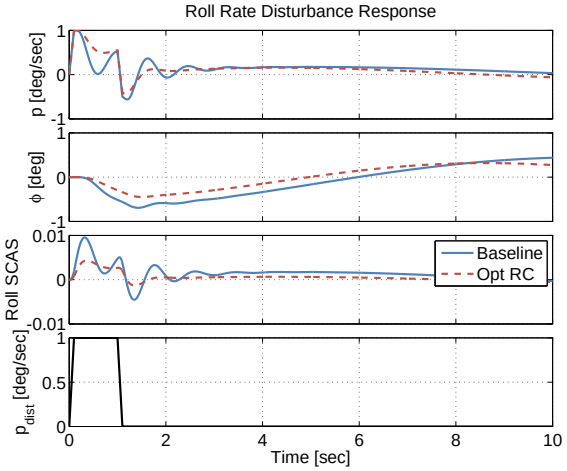

Fig. 16. Roll rate disturbance pulse response for the baseline and optimized RC gain configurations

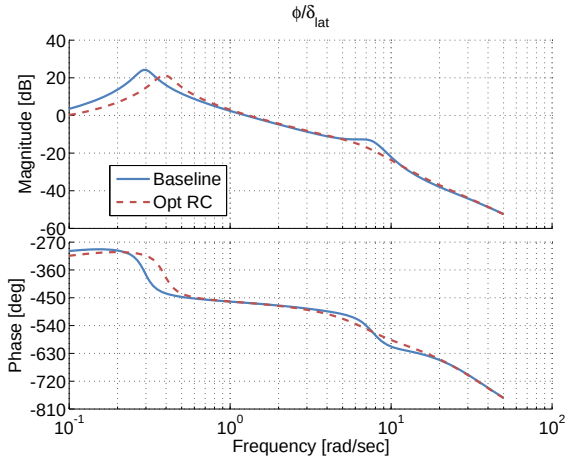

Fig. 17. Lateral closed-loop response for the baseline and optimized RC gain configurations

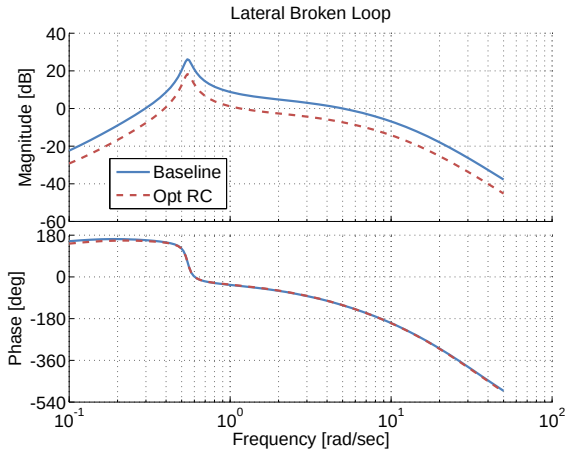

Fig. 18. Lateral broke-loop response for the baseline and optimized RC gain configurations

crease in values of the rate gain can be seen in Figures 20(a) and 20(b), respectively, as discussed in (Ref. 10). Finally, the increasing values of the feed forward stick gain can be seen for the "Qk" family of designs in Figure 20(c).

Indicated on the figures are the designs selected to be carried on to Phase 2 of flight testing, the control law comparison and down select. A "Lo" design with a roll attitude DRB of 0.99 rad/sec, a crossover of 2.3 rad/sec and a bandwidth of 4.0 rad/sec, a "Hi"design with a DRB of 1.09 rad/sec, a crossover of 2.8 rad/sec, and a bandwidth of 4.4 rad/sec, and "Qk"design with a DRB of 1.05 rad/sec, a crossover of 2.5 rad/sec, and a bandwidth of 4.0 rad/sec. These designs were selected for their high values of stability margins and damping and good DRB.

Table 5 lists the values of the roll axis handling qualities for the baseline and three short-term ACAH designs. Figures 21 through 26 show time- and frequency-domain comparisons between the two short-term ACAH designs. Figure 21 shows the larger roll rate generated by the "Qk" design versus the "Lo" and "Hi" designs. It also shows the increase in SCAS activity. This is also evident for both a roll rate and roll attitude disturbance pulse response in Figures 22 and 23, respectively. Figure 24 shows a comparison of the closed-loop roll attitude response of the three configurations. The higher DRB and associated higher DRP of the "Hi" response as compared to the "Lo" and "Qk" responses can be seen in Figure 25. Finally, the higher crossover of the "Hi" response and lower stability margin can be seen in Figure 26.

In the pitch axis, a single family of designs was generated. Two configurations were chosen, a "Lo" design with a pitch attitude DRB of 0.6 rad/sec, a crossover of 1.7 rad/sec and a bandwidth of 2.0 rad/sec and a "Hi"design with a DRB of 0.7 rad/sec, a crossover of 2.1 rad/sec, and a bandwidth of 2.2 rad/sec. Table 6 lists the values of the pitch axis handling qualities for the baseline and two short-term ACAH designs.

Improved Yaw SCAS and Heading Hold

The approach to improving the yaw SCAS was the same as described for the pitch and roll optimized RC designs. The objectives were to increase the stability margins and damping while reducing the crossover frequency. Table 7 lists the values of the specifications for the baseline and the optimized yaw SCAS design. The improved design has a lower crossover frequency and higher gain margin with better damping characteristics to provide more precise heading control with less overshoot.

The heading hold mode is implemented through both the yaw SCAS actuator and a separate yaw trim motor that is rate limited to about 10 %/sec. Commands from the heading hold mode continuously drive the yaw SCAS which is limited to $\pm$10% authority and pass through a deadband to drive the trim motor with 100% authority. Small commands result in SCAS inputs only while large commands result in both SCAS and trim inputs simultaneously. The approach to improving the heading hold performance was to increase the DRB while maintaining sufficient stability margin. Table 8 lists the specification values for the improved heading hold design. The improved yaw SCAS and heading hold designs were used in conjunction with all the improved lateral and longitudinal design cases during the piloted evaluations.

Table 7. Directional Handling Qualities Comparison

	Baseline	Optimized
ω_c [rad/sec]	4.0	3.0
PM [rad/sec]	82.9	73.7
GM [dB]	5.6	10.6
BW_{phase} [rad/sec]	2.1	2.0
BW_{gain} [rad/sec]	3.5	2.8
ζ [-]	0.23	0.65
DRB [rad/sec]	3.6	2.6
DRP [dB]	5.5	3.4

Table 8. Heading Hold Handling Qualities Comparison

	Baseline	Optimized
ω_c [rad/sec]	5.8	3.7
PM [rad/sec]	34.9	47.8
GM [dB]	3.7	7.6
ζ [-]	0.24	0.68
DRB [rad/sec]	0.78	0.95
DRP [dB]	2.2	3.2

Handling Qualities Flight Testing

To assess the optimized gains qualitatively, a limited flight test (4.6 hours) was conducted in the day (GVE) and at night (DVE). Two experienced experimental test pilots performed back-to-back comparisons of the baseline aircraft (RC) versus the down-selected optimized gain set (short-term ACAH) while performing the Hover, Acceleration/Deceleration, and Sidestep flight test maneuvers or Mission Task Elements (MTEs) from ADS-33E (Ref. 6). For the GVE, only the Hover maneuver was evaluated. The DVE flights were performed at night, with the evaluation pilots using NVGs. To achieve a Usable Cue Environment of two (UCE = 2), the NVGs were degraded with neutral density filters to provide a visual acuity of about 20/70 (Ref. 14). The flight test assessment was conducted at Courtland Airport, Courtland, AL (Figure 27). Winds during testing ranged from moderate to light.

The Aviation Flight Test Directorate (AFTD) provided mobile telemetry that allowed assessment and comparison of aircraft states with the MTE performance standards.

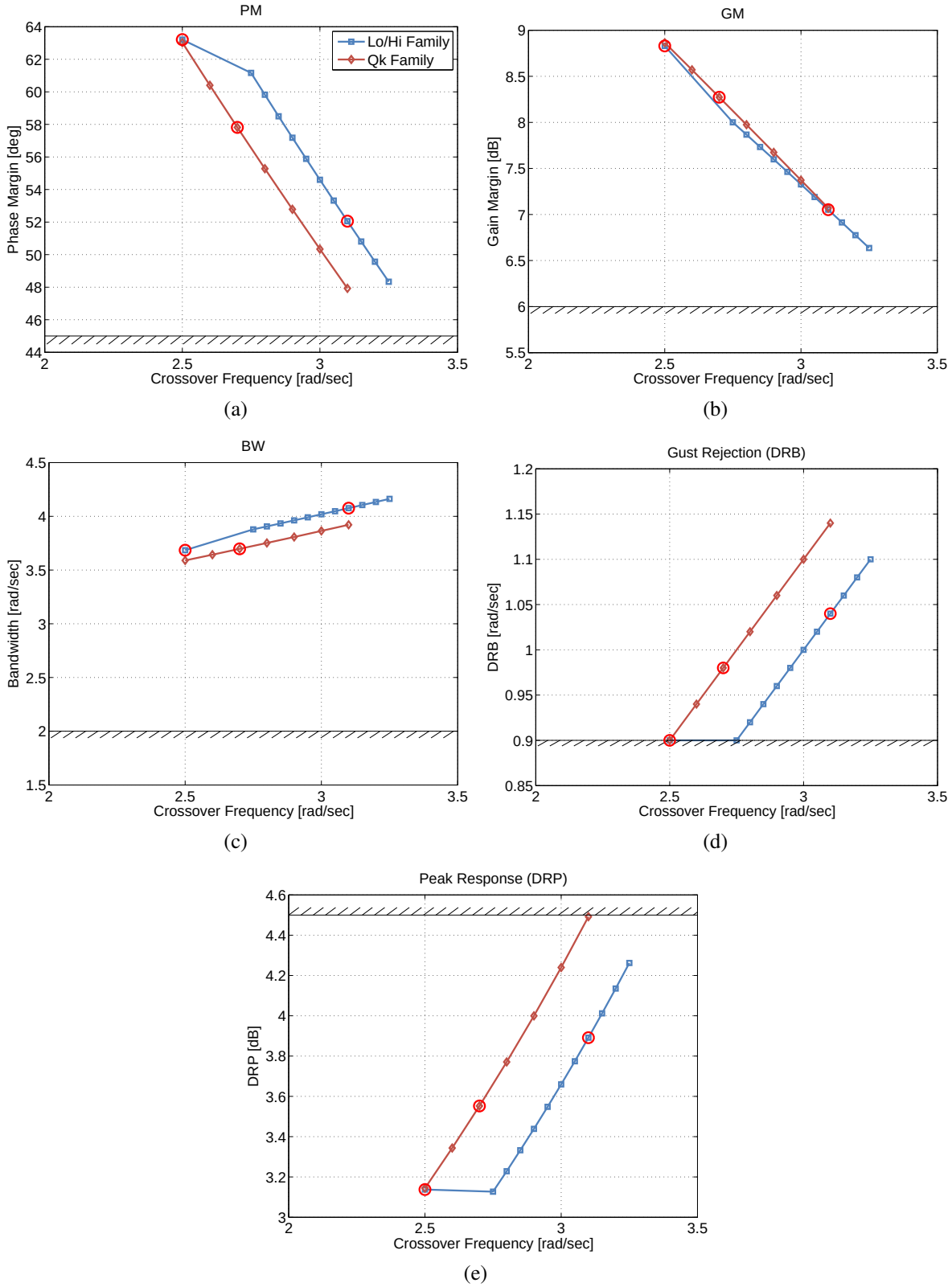

Fig. 19. (a) Phase margin, (b) gain margin, (c) bandwidth, (d) DRB, and (e) DRP, for the two short-term ACAH families of optimized designs versus crossover frequency. The selected "Lo" (left), "Hi" (right), and "Qk" (middle) cases are circled

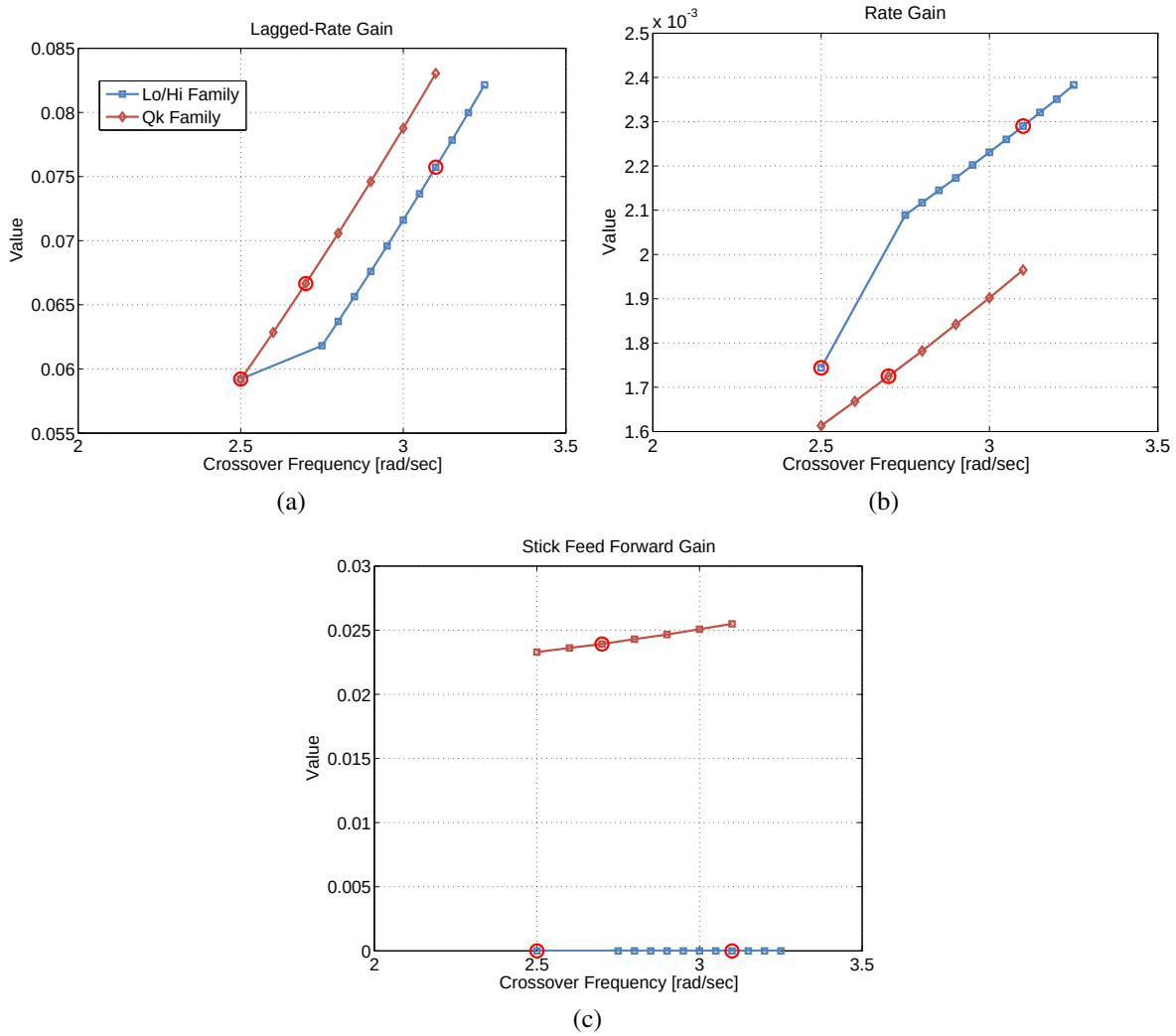

Fig. 20. **(a) Lagged-rate gain, (b) rate gain, and (c) stick feed forward gain for the two short-term ACAH families of optimized designs versus crossover frequency. The selected "Lo" (left), "Hi" (right), and "Qk" (middle) cases are circled**

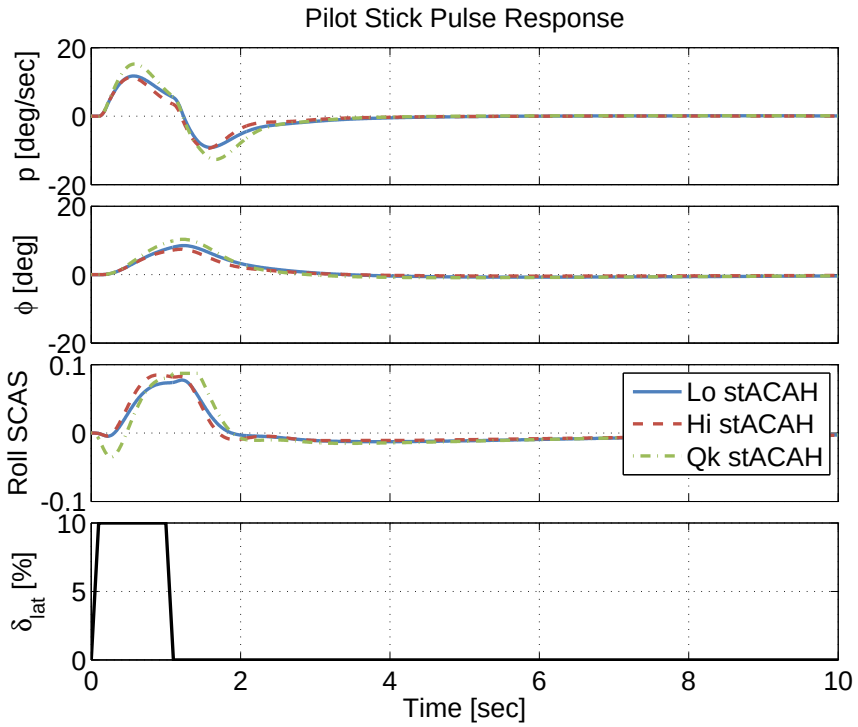

Fig. 21. Lateral pilot stick pulse response for the "Lo," "Hi," and "Qk" short-term ACAH gain configurations

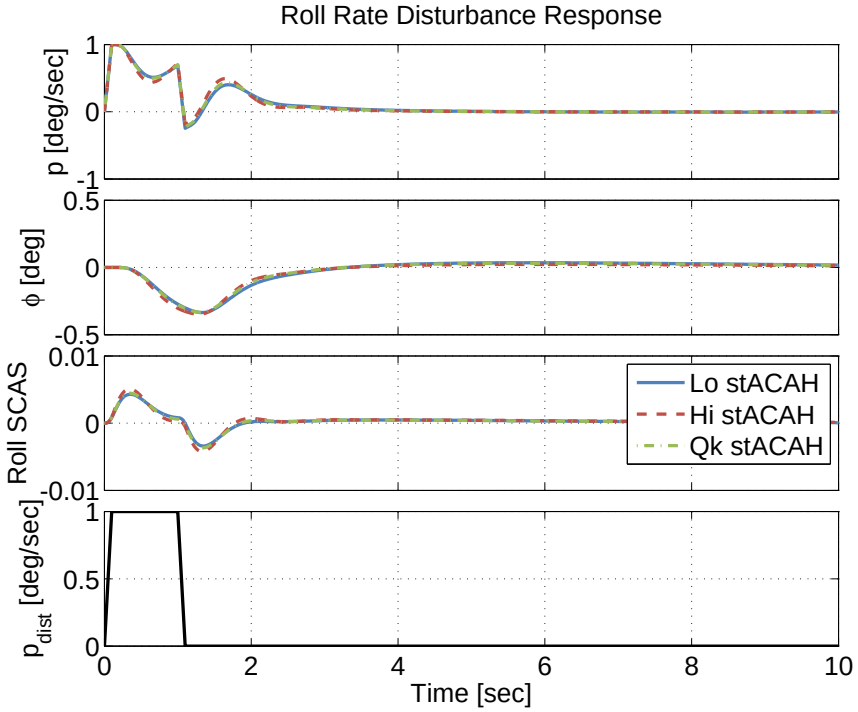

Fig. 22. Roll rate disturbance pulse response for the "Lo," "Hi," and "Qk" short-term ACAH gain configurations

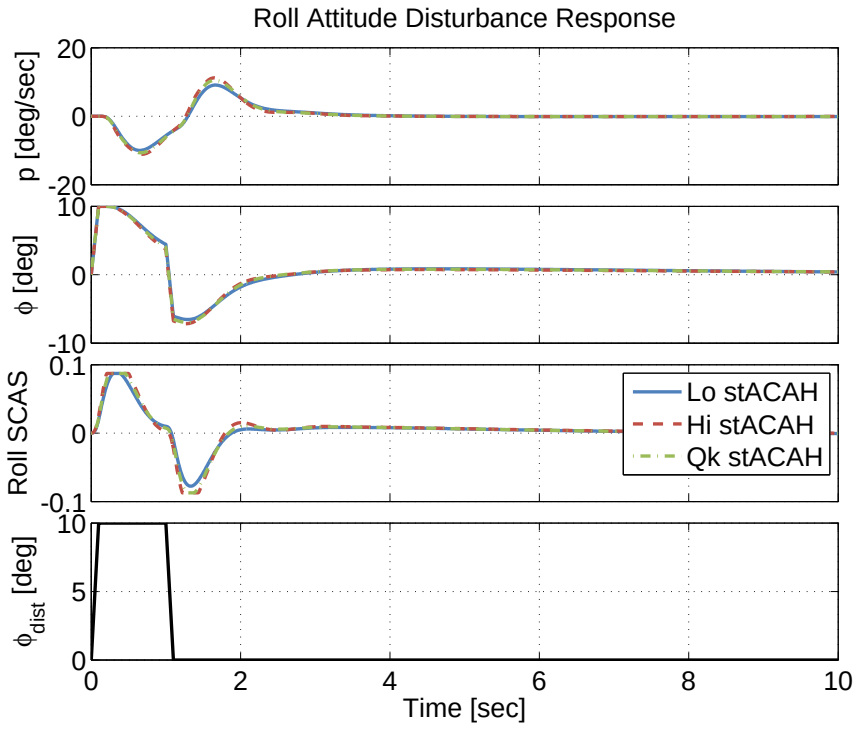

Fig. 23. Roll attitude disturbance pulse response for the "Lo," "Hi," and "Qk" short-term ACAH gain configuration

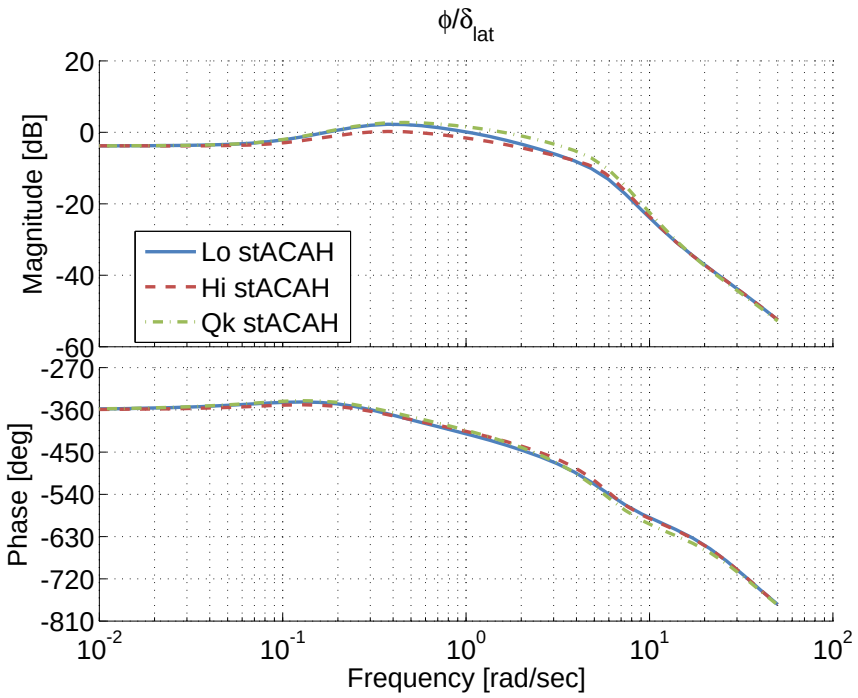

Fig. 24. Lateral closed-loop response for the "Lo," "Hi," and "Qk" short-term ACAH gain configurations

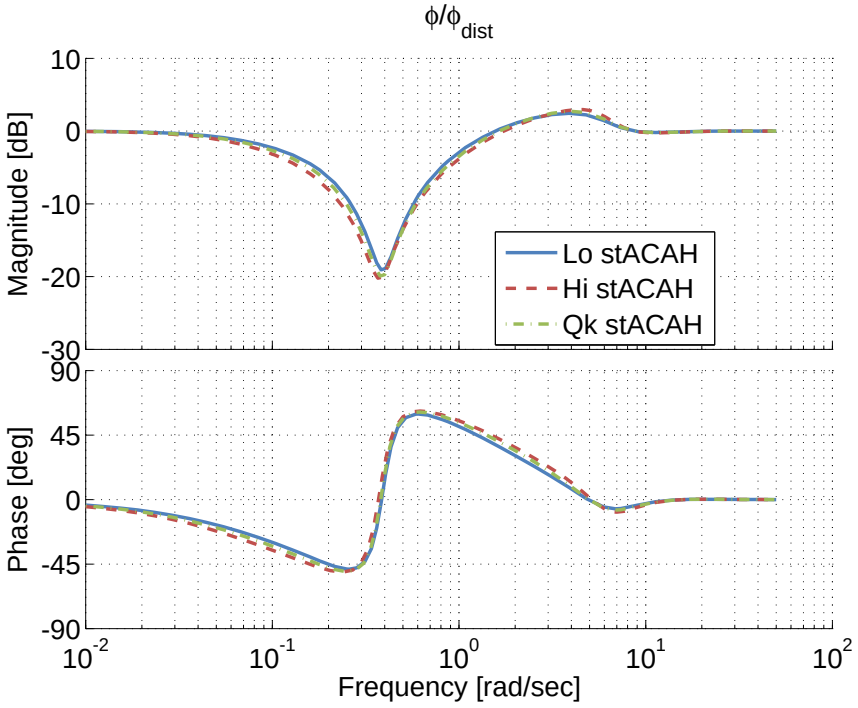

Fig. 25. Lateral disturbance response for the "Lo," "Hi," and "Qk" short-term ACAH gain configurations

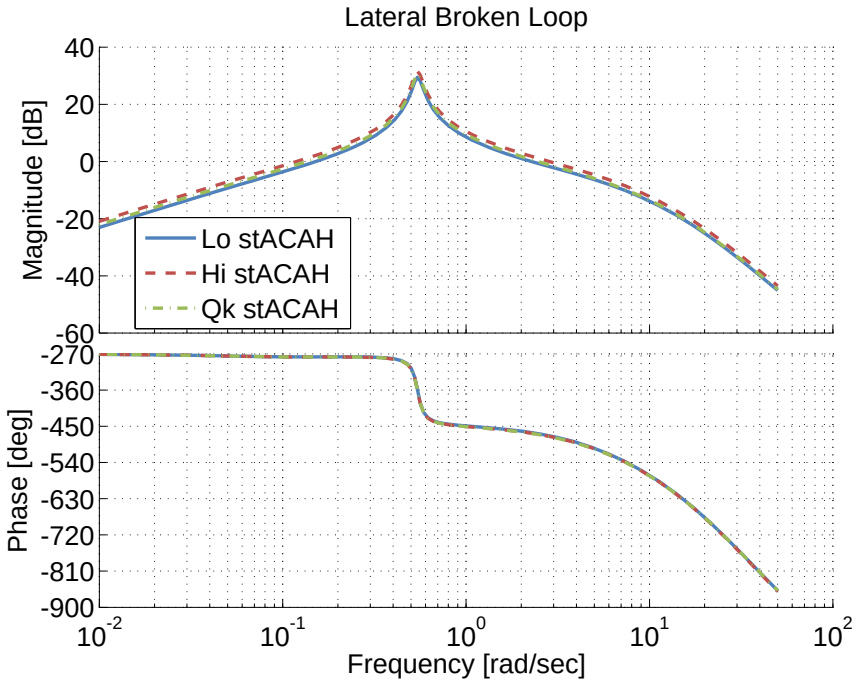

Fig. 26. Lateral broke-loop response for the "Lo," "Hi," and "Qk" short-term ACAH gain configurations

Fig. 27. Courtland Airport, Courtland, AL

Mission Task Elements

The Hover maneuver assesses the ability to transition from translating flight (6-10 kts) to a stabilized hover with a reasonable amount of aggressiveness and precision, maintaining precise position, heading, and altitude. Following the translation and transition to a stable hover, the pilot is to maintain a precise hover position ($\pm$3 ft) for 30 seconds.

The Acceleration/Deceleration maneuver assesses the pitch and heave axes during aggressive maneuvering, and checks for undesirable coupling, control harmony, and overly complex power management.

The Sidestep maneuver assesses the lateral-directional characteristics during aggressive maneuvering, and checks for undesirable inter-axis coupling and the ability to coordinate bank angle and collective to hold a constant altitude.

Results

Down Select Flight During the down select flight, pilots flew the Hover, Acceleration/Deceleration, and Sidestep MTEs (Ref. 6) with the different gains sets and gave qualitative feedback. This was also the only phase of flight testing that the Optimized RC gain set was tested. For the Optimized RC configuration, pilots commented that the roll axis was "damped" and "predictable." During the Hover MTE, pilots commented that it was easier to capture the hover, which took only one to two cyclic inputs, as opposed to three to four for the baseline configuration. Pilots also commented on a lower workload during the Acceleration/Deceleration and Sidestep MTEs and an easier ability to maintain lateral speed versus the baseline configuration. This is consistent with the significantly higher damping of the Optimized RC configuration over the baseline.

For the short-term ACAH designs, the pilots selected the "Qk" design in roll, because it was more stable than the baseline during the hover MTE, "roll maintenance was easier," and it was the "best for hover capture" out of all of the short-term ACAH configurations. Pilots commented that the "Lo" pitch axis design was "more stable," "more damped," and "more predictable" than the baseline. Therefore, the short-term ACAH design which was carried on to the formal handling qualities assessment was the "Qk" roll gains and the "Lo" pitch gains.

All optimized SCAS gains sets used the same optimized yaw gains. Pilots commented that heading was "more stable" during the Hover MTE. Further comments on the yaw axis were better and more predictable heading capture with less tendency to overshoot than the baseline design.

Formal Handling Qualities Evaluation (GVE and DVE) During the GVE evaluations, the Hover MTE only was flown. The winds were a headwind, nearly aligned with the heading of the aircraft, and ranged from 12-21 kts. Results for the GVE evaluations show the optimized gain set (short-term ACAH) to be more stable with less control inputs during the 30 second hover portion of the maneuver than the baseline aircraft (RC). Pilots commented that for portions of the 30 second hover, the controls remained nearly fixed resulting in a noticeable improvement and a workload reduction (HQR 3). Conversely, the baseline aircraft required continuous small control inputs to maintain position (HQR 4). Figure 28 shows the pilot HQRs for the Hover MTE in the GVE. The HQRs show a significant improvement from Level 2 to Level 1 for the optimized gain set over the baseline aircraft. Figure 29 shows the RMS of the lateral and longitudinal cyclic stick during the 30 second hover portion of the GVE Hover MTE. RMS values were calculated from the power spectral density spectrum of the stick percent deflections. There is a clear reduction in stick activity for the short-term ACAH configuration as compared to the baseline.

During the DVE evaluations, the winds shifted to 60-90 deg from the aircraft heading and were around 12 kts. Results for the DVE evaluations show similar improvement to the GVE results for the optimized gain set compared to the baseline aircraft. Overall workload was increased due to the winds (unpredictable heading control) and the night, i.e., with the reduction in peripheral vision due to NVGs, the pilot is required to frequently rotate his head a full 90 degrees between the forward cues and the cues to side. For the baseline aircraft HQR 5 and 6 were provided. For the optimized gain set two HQR 4s were provided. The major difference was due to the hover station keeping, the translation part of the task was rated as the same between the two configurations. Pilots commented that optimized gain set would also likely reduce workload during landings. Figure 30 shows the pilot HQRs for the Hover MTE in the DVE. Figure 31 shows the RMS of the lateral and longitudinal cyclic stick during the 30 second hover portion of the DVE Hover MTE. It shows that in the DVE, pilots were working harder overall to maintain the hover, but in the short-term ACAH configuration, the RMS was back down to nearly the GVE levels.

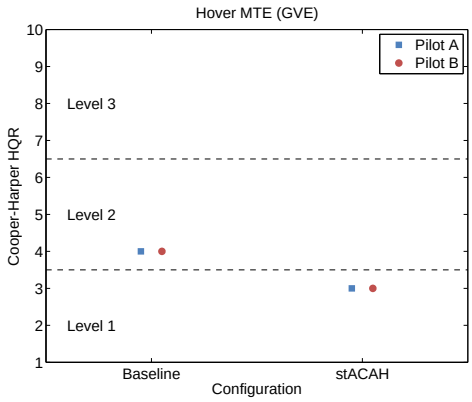

Fig. 28. Pilot HQRs for the Hover MTE in the GVE for the two configurations flown (baseline versus Optimized short-term ACAH)

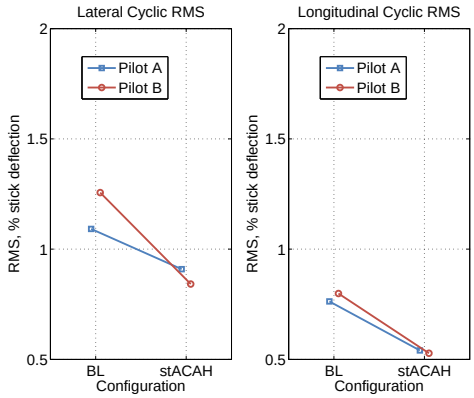

Fig. 29. Lateral (left) and longitudinal (right) cyclic stick RMS during the Hover MTE in the GVE for the two configurations flown (baseline versus Optimized short-term ACAH)

Pilot ratings from the Acceleration/Deceleration and Sidestep maneuvers were the same between the baseline aircraft and the optimized gain set (HQR 4). These results agree with (Ref. 15), which shows that a well designed ACAH system does not degrade agility.

Conclusions

1. The identified simple transfer function models and six degree-of-freedom state-space model accurately characterize the OH-58D bare-airframe responses for inputs at the swashplate. Carefully validated models of the mechanical mixing system and flight control system, as well as the integrated closed- and broken-loop responses were key to the rapid and successful flight test development of new control laws. These models and the frequency sweep data can also provide a solid basis for future simulation model development.

2. The existing limited authority SCAS architecture of the OH-58D was optimized to achieve an improved RC system that meets Level 1 ADS-33E handling qualities

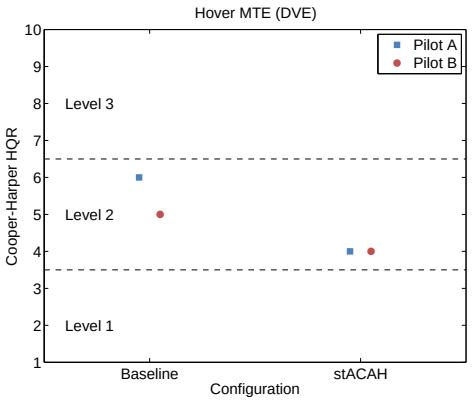

Fig. 30. Pilot HQRs for the Hover MTE in the DVE for the two configurations flown (baseline versus Optimized short-term ACAH)

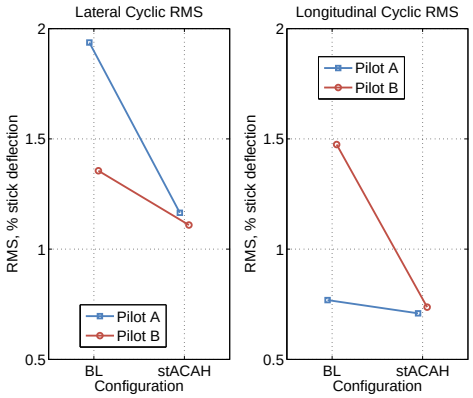

Fig. 31. Lateral (left) and longitudinal (right) cyclic stick RMS during the Hover MTE in the DVE for the two configurations flown (baseline versus Optimized short-term ACAH)

requirements and exhibits a better damped response. Pilots commented that the optimized RC system afforded lower workload and better pitch-pointing precision than the existing (baseline) rate SCAS.

3. An optimized short-term ACAH configuration provided better handling qualities than the baseline SCAS in both day (GVE) and night (DVE) during the Hover MTE. This configuration meets the ADS-33E requirement for an ACAH response type in the DVE *for the short-term response only* due to the requirement to maintain the current SCAS architecture, which lacks a pure attitude feedback.

4. During the more dynamic maneuvers, i.e. the Sidestep, Acceleration/Decelation, and the run in to the Hover task, pilots did not notice a significant difference between the baseline and short-term ACAH designs. This suggests that there is no significant loss of agility while performing these MTEs with the short-term ACAH design.

References

[1]Robinson, D., Brunson, K., Davis, A., Klase, S., Garrett, E., and Kelly, C., "OH-58D(R) Stability and Control Augmentation System Optimization," DTC Project No. 4-AI-130-58D-077/KF, November 2003.

[2]Anon., "USAACE Info Paper TCM-RA KW CASUP," Concepts and Requirements Directorate, United States Army Aviation Center of Excellence, March 2010.

[3]Couch, M. and Lindell, D., "Study on Rotorcraft Safety and Survivability," presented at the American Helicopter Society 66th Annual Forum, Phoenix, AZ, May 2010.

[4]Einthoven, P., Miller, D., Irwin, J., McCurdy, B., Bender, J., Blanken, C., and Lawler, M., "Development of Control Laws for the Chinook Digital AFCS Program," presented at the American Helicopter Society 62nd Annual Forum, Phoenix, AZ, May 2006.

[5]Fletcher, J. W., Lusardi, J. A., Moralez, E., Robinson, D. E., Arterburn, D. R., Cherepinsky, I., Driscoll, J., Morse, C. S., and Kalinowski, K. F., "UH-60M Upgrade Fly-By-Wire Flight Control Risk Reduction using the RASCAL JUH-60A In-Flight Simulator," presented at the American Helicopter Society Annual Forum , Montreal, Canada, April 2008.

[6]Anon., "Handling Qualities Requirements for Military Rotorcraft," Aeronautical Design Standard-33 (ADS-33E-PRF), US Army Aviation and Missile Command, March 2000.

[7]Tischler, M. B. and Remple, R. K., *Aircraft and Rotorcraft System Identification: Engineering Methods and Flight Test Examples*, AIAA, 2006.

[8]Ham, J. A., Gardner, C. K., and Tischler, M. B., "Flight Testing and Frequency Domain Analysis for Rotorcraft Handling Qualities Characteristics," presented at the American Helicopter Society Specialists' Meeting, San Francisco, CA, January 1993.

[9]Heffley, R. K., Bourne, S. M., Curtis., H. C., Hindson, W. S., and Hess, R. A., "Study of Helicopter Roll Control Effectiveness Criteria," NASA CR 177404, April 1986.

[10]Tischler, M. B., Ivler, C. M., Mansur, M. H., Cheung, K. K., Berger, T., and Berrios, M., "Handling-Qualities Optimization and Trade-offs in Rotorcraft Flight Control Design," presented at the Rotorcraft Handling Qualities Conference, University of Liverpool, UK, Novebmer 2008.

[11]Anon., "Flight Control Systems - Design, Installation and Test of Piloted Aircraft, General Specifications for,," MIL-DTL-9490E, U.S. Air Force, April 2008.

[12]Christensen, K. T., Campbell, K. G., Griffith, C. D., Ivler, C. M., Tischler, M. B., and Harding, J. W., "Flight Control Development for the ARH-70 Armed Reconnaissance Helicopter Program," presented at the American Helicopter Society 63th Annual Forum, Virginia Beach, VA, May 2007.

[13]Mansur, M. H., Lusardi, J. A., Tischler, M. B., and Berger, T., "Achieving the Best Compromise between Stability Margins and Disturbance Rejection Performance," presented at the American Helicopter Society 65th Annual Forum, Grapevine, TX, May 2009.

[14]Blanken, C. L., Hoh, R. H., Mitchell, D. G., and Key, D. L., "Test Guide for ADS-33E-PRF," US Army RDECOM special report AMR-AF-08-07, July 2008.

[15]Fujizawa, B. T., Lusardi, J. A., Tischler, M. B., Braddom, S. R., and Jeram, G. J., "Response Type Tradeoffs in Helicopter Handling Qualities for the GVE," presented at the American Helicopter Society Annual Forum , Virginia Beach, VA, May 2011.